Research Article | Vol. 29, No. 24 / 22 Nov 2021 / Optics Express 40345
Optics EXPRESS

Brillouin-like amplification in rare-earth-doped optical fibers

A. A. Fotiadi,[1,2,3,*] D. A. Korobko,[1] I. O. Zolotovskii,[1] and J. R. Taylor[4]

[1] Ulyanovsk State University, 42 Leo Tolstoy Street, Ulyanovsk, 432970, Russian Federation
[2] Ioffe Physical-Technical Institute, RAS, St. Petersburg 194021, Russian Federation
[3] Electromagnetism and Telecommunication Department, University of Mons, Mons, B-7000, Belgium
[4] Femtosecond Optics Group, Department of Physics, Imperial College London, London SW7, UK
[*] Andrei.Fotiadi@gmail.com

Abstract: We present a theoretical formalism to describe the amplification of two monochromatic waves counter-propagating in a rare-earth-doped optical fiber amplifier. Interaction of the waves through a dynamical population inversion grating inscribed in the active fiber by the waves during their amplification results in a strong power transfer from one wave to another providing a preferable amplification of one wave at the expense of another. In this sense, the effect is similar to stimulated Brillouin scattering and is expected to be observed with both pumped and unpumped rare-earth-doped fibers possessing a finite polarizability difference between the excited and ground states.

1. Introduction

In contrast to the stationary Fiber Bragg Gratings (FBG), the dynamical gratings (DG) can be implemented only temporarily in an optical fiber. The light-induced dynamic gratings are inscribed through the interaction between the optical medium and an interference pattern formed by a number of coherent light waves [1]. A physical mechanism responsible for dynamic grating inscription strongly depends on the media properties. Acoustic waves enhanced by a stimulated Brillouin scattering (SBS) in optical fibers create a refractive index grating known as Brillouin dynamic grating (BDG) that has recently emerged as a flexible tool for optical processing, microwave photonics and distributed sensing [2–7]. The population inversion dynamical gratings (PIDG) inscribed by counterpropagating optical waves in rare-earth-doped fibers are responsible for rather slow or even stationary dynamical effects [8]. In standing-wave lasers, spatial hole burning induces a static grating of the population inversion, enabling multimode operation with several independent lasing modes [9]. In open-cavity fiber lasers, the slowly-moving PIDGs inscribed in an active medium by intracavity radiation have a reverse effect on the inscribing waves via feedback they provide leading to so called "mode-pulse" laser operation different from mode-locked and Q-switched laser regimes [10,11]. Among other PIDG applications are adaptive interferometry and nonlinear filtering enabling narrowband operation of semiconductor and fiber laser configurations [12–16].

Brillouin amplification, the most prominent effect implemented with BDG, enables exponential narrowband gain that is Stokes-shifted by some value in the GHz range [17,18]. In this process, the interaction of the counterpropagating pump and Stokes waves through a BDG they produce causes an increase of the Stokes-shifted wave amplitude and decrease of the pump wave amplitude during their propagation through the fiber. Here, we report on a similar effect that could be implemented in rare-earth-doped fibers with the PIDG. The effect is the most pronounced in a bidirectional rare-earth-doped optical fiber amplifier. In general, the fiber depicted in Fig. 1 exhibits the population inversion gain $G(z)$ caused by some external pump field. Two monochromatic optical signal waves with amplitudes E_S^+ and E_S^- are introduced into the fiber from

#437424 https://doi.org/10.1364/OE.437424
Journal © 2021 Received 8 Jul 2021; revised 4 Oct 2021; accepted 21 Oct 2021; published 18 Nov 2021

Optics EXPRESS

opposite ends and experience amplification (if the fiber is pumped) or attenuation (if the fiber is unpumped) as they propagate through the fiber. The signal waves are coherent on a sub-kHz level and slightly detuned. In terms commonly accepted in SBS these counterpropagating signal waves correspond to what is referred to as "pump" and "Stokes" waves. However, in contrast to the Brillouin process, their interference inside the rare-earth-doped fiber creates not acoustic, but the population inversion dynamical gain grating described by the amplitude $g(z)$. Then interaction between the signal waves and created PIDG causes a strong power transfer from one signal wave to another.

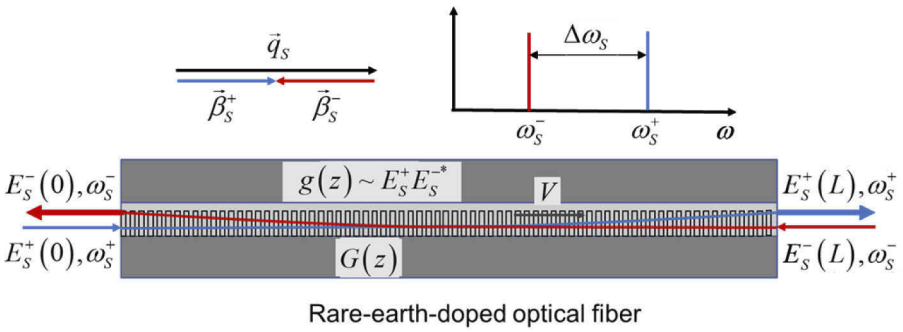

Fig. 1. Amplification of counter-propagating optical signal waves in a rare-earth doped optical fiber. $E_S^{\pm}(z)$ are signal wave amplitudes, $\omega_S^{\pm}$ are signal wave frequencies, $\Delta\omega_S = \omega_S^+ - \omega_S^-$ is detuning of the signal waves, $G(z)$ is population inversion gain caused by some external pump field (it is not shown), $g(z)$ is the amplitude of the population inversion gain gratings created by the interference of signal waves, $\vec{\beta}_S^{\pm}$ and $\vec{q}_S$ are the wave vectors of the signal waves and PIDG, respectively, V is the PIDG group velocity, L is the fiber length.

Like Brillouin amplification, the effect exhibits a strong resonance dependence on the frequency detuning $\Delta\omega_S = \omega_S^+ - \omega_S^-$, where $\omega_S^{\pm}$ denotes the frequencies of the signal waves and the dynamical wave equations are similar to the SBS equations [19–21]. At each fiber point the most effective power transfer is achieved at the frequency detuning $\Delta\omega_S$ matching the local grating relaxation time τ_G that is determined by the doping rare-earth-ion lifetime T and decreases with an increase of operating powers. In contrast to SBS, the power transfer in the rare-earth-doped fibers can occur either to the wave with higher (anti-Stokes) or lower (Stokes) frequency. Anti-Stokes wave amplification dominates in pumped fibers, while amplification of the Stokes wave could occur in fibers without pumping. In this paper, we give a clear physical insight into the Brillouin-like amplification in rare-earth doped optical fibers and present important details of the fiber model. In particular, the equations reproducing inscription of the population inversion gratings in the fiber by counterpropagating monochromatic optical signals and the dynamics of the reverse effect the inscribed gratings produced on the amplification process are derived and presented in terms of standard fiber specifications.

2. Mathematical model

In our consideration the rare-earth-doped optical fiber shown in Fig. 1 is single-mode and pumped by some external pump field. The population inversion provides an amplification to the monochromatic optical signal waves with amplitudes E_S^+ and E_S^- counterpropagating through the fiber. Without a loss of generality, we can assume in this paper that the fiber under consideration is an ytterbium-doped silica optical fiber, the pumping source wavelength is $\lambda_P \sim 975nm$ and the optical signal wavelengths are around $\lambda_S \sim 1060nm$. Silica glass, the most common material for manufacturing fibers, is a good host for Yb-ions [22]. The spectroscopy of the Yb-ion

Optics EXPRESS

shown in Fig. 2(a) is simple compared to other rare-earth ions. For amplification in the optical spectrum range, only two-level manifolds are important: the ground-state manifold ($^2F_{7/2}$) and the excited-state manifold ($^2F_{5/2}$). Although they consist of four and three sublevels, respectively, the transitions between sublevels are smoothed due to strong homogeneous and inhomogeneous broadening. Yb-doped fibers are able to produce optical gain over a very broad wavelength range spanning from 975 to 1200 nm with a range of possible pump wavelengths from 860 nm to 1150 nm (Fig. 2(b)). A number of pronounced laser effects governed by the population inversion mechanism have been observed in single-mode Yb-doped optical fibers under resonant diode pumping at 975 nm. Importantly, similar to other rare-earth-doped fibers the Yb-doped fibers are subjected to electronic refractive index change (RIC) effect that is the side effect of the population inversion mechanism [23,24]. Commonly, the two-level population laser model [25,26] is enough to provide an accurate interpretation to these effects as confirmed by multiple experimental observations. Here, we use the two-level population laser model to explore the Brillouin-like amplification in rare-earth-doped fibers and to demonstrate its spectral and dynamical properties.

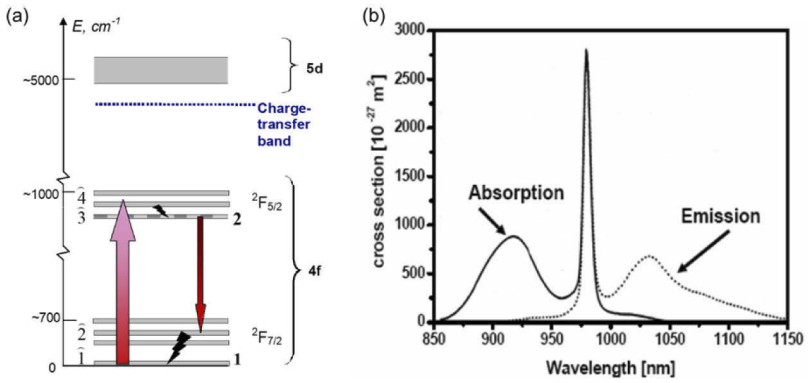

Fig. 2. The atomic manifold level system (a) and emission and absorption cross section of ytterbium in silica host (b). 1, 2 and $\hat{1}$, $\hat{2}$, $\hat{3}$, $\hat{4}$ indicate the levels for two- and four- level laser models, respectively.

Mathematically, we consider amplification of two monochromatic optical signals $E_S^{\pm}\exp[i(\omega_S^{\pm}t \mp \beta_S^{\pm}z)]$ with the propagation constants $\beta_S^{\pm}$ propagating through the fiber in positive (+) and negative (-) directions, respectively. An external pumping (one- or two- directional) creates both the population density of Yb-ions in the excited state $N_2(z)$ and corresponding optical gain factor $G(z)$ smoothly distributed over the fiber. Due to the optical gain $G(z)$ the amplitudes $E_S^{\pm}$ increase as the optical signals propagate through the fiber.

On the other hand, the superposition of the amplified counter-propagating optical fields inside the fiber forms an interference pattern $I(t,x) \sim E_S^{+}E_S^{-*}\exp[i(\Delta\omega_S t - q_S z)]$ covering the whole fiber length, where the frequency difference is $\Delta\omega_S \equiv \omega_S^{+}-\omega_S^{-}$, the wavenumber is $q_S = \beta_S^{+}+\beta_S^{-}\approx 2\tilde{\omega}_S n/c$ and $\tilde{\omega}_S \equiv (\omega_S^{+}+\omega_S^{-})/2$. The interference pattern $I(t,z)$ produces a spatial longitudinal modulation of the population density $N_2(z)$ in the fiber core $\delta N_2(t,z) \sim I(t,z)$ resulting in a similar modulation of the optical gain $\delta G(t,z) \sim I(t,z)$. Due to the electronic RIC effect mentioned above, the modulation of the optical gain $\delta G(t,z)$ is followed by the identical modulation of the fiber core refractive index $\delta n(t,z) \sim I(t,z)$. This bundle of quantities combined as $\Gamma = (\delta G + ik^0\delta n)\exp[i(\Delta\omega_S t - q_S z)]$ is referred to as the population inversion dynamical grating (PIDG). Here, the first and second terms are known as the amplitude (gain) and phase dynamical gratings, respectively. In two-level approximation the Kramers - Kronig relation determining the RIC effect in rare-earth-doped fibers [23,24] gives the following expressions for

Optics EXPRESS

the grating amplitudes:

$$\begin{aligned} \delta G &= (\sigma_{21}^{(s)} + \sigma_{12}^{(s)})\rho_S(0)\delta N_2 \equiv Reg \\ k^0\delta n &= \frac{4\pi^2 {F_L}^2}{\lambda_S n_0}\Delta p_d \delta N_2 \equiv \mathrm{Im}g \end{aligned} \tag{1}$$

where $F_L = ({n_0}^2 + 2)/3$ is the Lorentz factor; n_0 is the unperturbed refractive index, $\sigma_{21}^{(s)}$ and $\sigma_{12}^{(s)}$, are the emission and absorption cross-sections at optical signal wavelengths, $\rho_S(r)$ is the normalized radial distribution of the signal power; $k^0 = 2\pi/\lambda_S$ is the signal wave number in vacuum; $\Delta p_d = p_2 - p_1$, p_1 and p_2 are the polarizabilities of the Yb-ions in the ground and excited states, respectively. From Eqs. (1), the ratio between the phase and gain grating amplitudes is fixed, since it is determined only by the operation wavelength λ_S and the polarizability difference Δp_d and does not depend on the operating powers:

$$\kappa \equiv \frac{\mathrm{Im}g(t,z)}{Reg(t,z)} = \frac{(2\pi F_L)^2}{\lambda_S[n_0(\sigma_{21}^{(s)} + \sigma_{12}^{(s)})\rho_S(0)]}\Delta p_d \tag{2}$$

It is a specific feature of the dynamical gratings inscribed through the population inversion mechanism. The polarizability difference Δp_d measured for Yb-doped fibers gives $\kappa = 2.7$ at $\lambda_S \sim 1060\ nm$[23].

When the optical signal waves propagate through the fiber amplifier their amplitudes are changed due to optical gain $G(z)$ and interaction with the PIDG $g(t,z)$. The equations describing the propagation of optical signals are derived in the Appendix A. The amplified optical waves always interact with the PIDG $g(t,z)$ they inscribe, since the Bragg conditions [17], $\Delta\omega_S \equiv \omega_S^+ - \omega_S^- = \Omega$, $\beta_S^+ + \beta_S^- = q_S$ are always satisfied. The process of grating inscription is governed by the set of rate equations derived in Appendix B. A self-consistent set of equations describing the Brillouin-like amplification in the rare-earth-doped fibers reads as:

$$\begin{aligned} &\left(\beta_1\frac{\partial}{\partial t} + \frac{\partial}{\partial z}\right)e_S^+ = \frac{(1-i\kappa)}{2}(\Lambda e_S^+ + g e_S^-) + i\kappa W_S e_S^+ \\ &\left(\beta_1\frac{\partial}{\partial t} - \frac{\partial}{\partial z}\right)e_S^- = \frac{(1-i\kappa)}{2}(\Lambda e_S^- + g^* e_S^+) + i\kappa W_S e_S^- \\ &\tau_G\frac{d\Lambda}{dt} = \frac{W_P p_P - (p_P+1)W_S}{(p_P + p_S + 1)} - \Lambda \\ &\tau_G\frac{dg}{dt} = -(1 + i\Delta\omega\tau_G)g - \frac{\Lambda}{(p_p + p_s + 1)}e_S^+ e_S^{-*} \\ &\frac{n_0}{c}\frac{\partial p_P^\pm}{\partial t} \pm \frac{\partial p_P^\pm}{\partial z} = s(\Lambda + W_S)p_P^\pm - \alpha_P p_P^\pm \end{aligned} \tag{3}$$

where $\tau_G = T/(p_P + p_S + 1)$ is the local population inversion rise time, $e_S = E_S^\pm/\sqrt{P_{S0}}$, $p_P^\pm = P_P^\pm/P_{P0}$, $p_S^\pm = E_S^\pm E_S^{\pm *}/P_{S0}$, $p_{P,S} = p_{P,S}^+ + p_{P,S}^-$, are optical fields and powers normalized to the corresponding saturation powers P_{S0} and P_{P0}; $\Lambda \equiv G - W_S$ is the net gain factor; W_P and W_S are the stimulated transition rates between the ground and excited states for ω_P and signal $\omega_S^\pm$ frequencies, respectively; T is the rare-earth ion lifetime, $s = P_{S0}\omega_P/P_{P0}\omega_S^\pm$, κ is the ratio between amplitudes of the phase and amplitude gratings (determined by the polarizability difference [23]).

In Eqs. (3), the first two equations describe propagation of two optical monochromatic waves through the fiber. In these two equations the first terms in brackets are responsible for amplification of the signals through the population inversion mechanism. The second terms describe interactions of the signal waves with the backward waves through the dynamical grating. The latter terms are similar to the corresponding terms in Brillouin equations and are responsible

Optics EXPRESS

for the Brillouin-like effect. The third equation describes the optical gain factor provided by the population inversion mechanism in the fiber. One can see that the rise time function τ_G determined by the Yb-ion lifetime T and all operating powers sets a pace to all transition processes in the system. Also, the function τ_G characterizes the local lifetime of dynamical grating governed by the fourth equation. One can see that, in contrast to the stationary fiber Bragg grating [27–29], the dynamical grating exists in the fiber only when the fiber is exposed to the interference pattern. Once exposure is terminated (or the interference pattern is shifted), the grating amplitude decays exponentially with the characteristic time τ_G referred to as the local grating lifetime. Specifically, for PIDG, the grating lifetime τ_G decreases with an increase of the operating powers. In this sense, higher operating powers support faster erase of the grating. One can see that the dynamical grating inscribed by the counterpropagating waves of equal frequencies ($\Delta\omega = 0$) is stationary (its position is fixed). Otherwise ($\Delta\omega \neq 0$), the interference pattern moves through the fiber in positive (if $\Delta\omega$>0) or negative (if $\Delta\omega$>0) direction with the velocity $V \approx c\Delta\omega/2\tilde{\omega}n$ inscribing the moving gratings. The moving gratings could be thought as a permanent process of the grating re-inscription: each time a new grating is inscribed at a new position, while the previous grating is erased. In these terms, the efficiency of the grating inscription (i.e., the grating amplitude) depends on the grating velocity V in relation to the grating period $\sim\pi c/\tilde{\omega}n$ divided by the grating lifetime τ_G. Inscription is most efficient for the stationary gratings ($V = 0$, $\Delta\omega = 0$) and becomes weak at $\Delta\omega\tau_G \sim \pi$, when the interference pattern is shifted by a half of the grating period for the grating lifetime. The last two equations in Eq. (3) are common equations from the two-level laser model [26,30] describing the dynamics of the pump powers. This dynamics has a minor effect on the Brillouin-like amplification but may complicate its observation. It is for this reason, an Yb-doped double-clad fiber possessing trivial pump dynamics is select here for numerical demonstration.

For steady-state power distributions over the fiber Eq. (3) is reduced to:

$$\frac{\partial}{\partial z}\ln p_S^{\pm} = \pm\Lambda\left[1 - \frac{\tau_G}{T}\frac{1}{1+(\Delta\omega\tau_G)^2}p_S^{-} \pm \frac{\tau_G}{T}\frac{\kappa\Delta\omega\tau_G}{1+(\Delta\omega\tau_G)^2}p_S^{-}\right] \tag{4}$$

providing the steady-state net gain Λ and the grating local lifetime τ_G as:

$$\begin{aligned}\Lambda &= \frac{W_P p_P - (p_P+1)W_S}{(p_P+p_S+1)}\\ \frac{\tau_G}{T} &= \frac{1}{(p_P+p_S+1)}\end{aligned} \tag{5}$$

3. Simulation results and discussion

In Eq. (4) the first term in the brackets is responsible for signal amplification through the population inversion mechanism. The second term describes a decrease of the gain due to the hole burning effect [31]. Its origin is the deconstructive interference of the wave passed through the grating and another wave reflected by the grating. The third term highlights the Brillouin-like effect, i.e., the effect of power transfer from one monochromatic wave to another through the interaction with the dynamical grating these two waves inscribe. Figure 3 shows the total gain spectrum decomposed into these three contributions at a fixed fiber point. The first mechanism does not depend on the frequency difference $\Delta\omega_S$. It dominates at $\Delta\omega_S = \infty$ when the contribution of two other mechanisms is negligible. The second mechanism (hole burning) is the most pronounced at $\Delta\omega_S = 0$ when the recorded dynamic grating is static (its velocity $V = c/2n\ \Delta\omega_S/\omega_S \rightarrow 0$) and the grating amplitude is maximal. In this case, the amplified wave and the optical wave reflected from the dynamic grating are strictly in antiphase and their coherent annihilation causes a decrease of the net amplification. The effect is symmetrical in respect to $\Delta\omega_S$ and, therefore, similarly influences both waves. With an increase of $|\Delta\omega_S|$>0, the velocity of the moving grating

Optics EXPRESS

increases and the grating amplitude decreases leading to mitigation of the hole burning effect. The effect described by the third term is caused by a phase part of the population inversion dynamic grating and is proportional to κ. It is asymmetrical in respect to $\Delta\omega_S$, i.e., the wave possessing higher frequency is always amplified at the expense of the wave possessing lower frequency. Similar to the SBS, the same gain (nonlinear loss) factor is responsible for the gain experienced by one wave and the nonlinear losses experienced by the second wave. Similar to SBS, the gain (nonlinear loss) increment of one wave is proportional to the power of the second wave. The effect is negligible in the limit cases of $\Delta\omega_S = \infty$ and $\Delta\omega_S = 0$, and is more pronounced at $\Delta\omega_S\tau_G \sim 1$. The combined action of all three mechanisms leads to a characteristic gain spectrum exhibiting resonant and anti-resonant peaks. The maximal and minimal gain frequencies are determined by $\Delta\omega_{S\max}\tau_G = \left(1+\sqrt{1+\kappa^2}\right)/\kappa$ and $\Delta\omega_{S\min}\tau_G = \left(-1+\sqrt{1+\kappa^2}\right)/\kappa$, respectively.

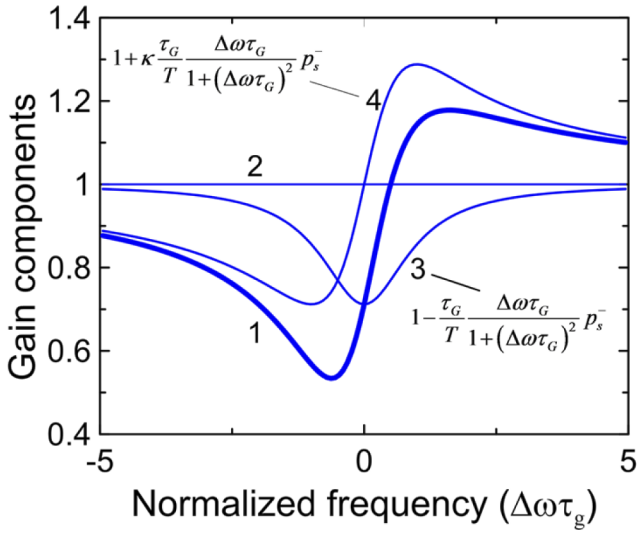

Fig. 3. Local gain spectrum for p^+ (curve 1). Contributions of terms in the brackets of Eq. (5): the first term responsible for uniform signal amplification due to the population inversion (curve 2); the first term and second term responsible for the hole burning effect (curve 3); the first term and the third term responsible for the Brillouin-like effect (curve 4). $p_S^+\tau_G/T = 0.3$ is taken for calculation.

The steady-state solution described by Eq. (4) (combined with Eq. (5) and last two equations in Eqs. (3) omitting derivatives in time) highlights the effect of the Brillouin-like amplification. The solution for a 25-cm-length Yb-doped fiber length has been obtained numerically using the Runge-Kutta algorithm. The boundary conditions are $P_S^+(0) = P_{Sin}^+$; $P_S^-(L) = P_{Sin}^-$;$P_P^+(0) = P_P^-(0) = P_{Pin}/2$, where P_{Sin}^+, P_{Sin}^-, P_{Pin} are the signal and pump input powers. The specific double-clad Yb-doped fiber parameters used in simulations are listed in Table 1.

Figure 4(a) shows typical steady-state power distributions of the interacting waves along the fiber at different values of $\Delta\omega_S$. The pump power is $P_{Pin} = 1.5W$ and the optical signal inputs are P_{Sin}^+=P_{Sin}^-=$1mW$. The curves calculated at $\Delta\omega_S = \infty$ describe the amplification of optical signals through the population inversion mechanism in the rare-earth optical amplifier. The counterpropagating optical signals experience amplification independently without mutual interaction. Thanks to symmetry of the setup and two-side pumping both optical signals starting from the same input power acquire the same total amplification equal to $P_S^+(L)/P_{Sin}^+$=$P_S^-(0)/P_{Sin}^-$=100. Comparing the curves obtained at $\Delta\omega_S = 0$ and $\Delta\omega_S = \infty$ one can see the hole-burning effect. The net amplification achieved at $\Delta\omega_S = 0$ is ~1.2 times lower (factor A) than that obtained in the

Optics EXPRESS

Table 1. Parameters of the Yb-doped fiber amplifier used for calculations

Symbol	Quantity	Value
λ_P	Pump wavelength	975 nm
λ_S	Optical signal wavelength	1060 nm
$\sigma_{12}^{(p)}$	Effective pump absorption cross sections	$2.69 \cdot 10^{-24} m^2$
$\sigma_{21}^{(p)}$	Effective pump emission cross sections	$2.97 \cdot 10^{-24} m^2$
$\sigma_{12}^{(s)}$	Effective signal absorption cross sections	$4.6 \cdot 10^{-27} m^2$
$\sigma_{21}^{(s)}$	Effective signal emission cross sections	$3.0 \cdot 10^{-25} cm^2$
N_{Yb}	Concentration of Yb ions in the fiber core	$10.4 \cdot 10^{19}$
r_P	Radius of the fiber inner cladding	$65 \cdot 10^{-6}$ m
r_S	Radius of the fiber core	$2.5 \cdot 10^{-6}$ m
T	Yb-ion lifetime in the excited state	$0.85 \cdot 10^{-3}$ s
Δp_d	Polarizability difference	$1.2 \cdot 10^{-32} cm^3$
F_L	Lorentz factor	1.42
κ	Ratio of phase and gain grating amplitudes	2.68

case of independent amplification of two waves ($\Delta\omega_S = \infty$). Both curves exhibit strong symmetry in respect to the midpoint of the fiber and $P_S^+(L)/P_{Sin}^+ = P_S^-(0)/P_{Sin}^- = 81.3$. A comparison of the curves obtained at $\Delta\omega_S = 0$ and $\Delta\omega_S/2\pi = 3.2 kHz$ ($\Delta\omega_S \tau_G$ is within the range of ~1.2-2.7 over the fiber length) highlights the Brillouin-like effect providing stronger amplification to the wave possessing higher frequency at expense of the wave possessing lower frequency. One can see that the output power of the signal at higher frequency is 1.53 times higher than its output power without interaction (at $\Delta\omega_S = \infty$) (factor B) and it is 4.25 times higher than the output power of the signal at lower frequency (factor C). The factors A, B, and C are introduced here as numbers characterizing efficiency of the hole-burning effect (factor A), the Brillouin-like amplification effect (factor C), and superposition of them (factor B). In fact, $\ln A$, $\ln C$, and $\ln B$ are expressed as integrals of the second, third, and sum of second and third terms of the Eq. (4) over the fiber length, respectively. The factor A is equal to the inverted factor B taken at $\Delta\omega_S = 0$.

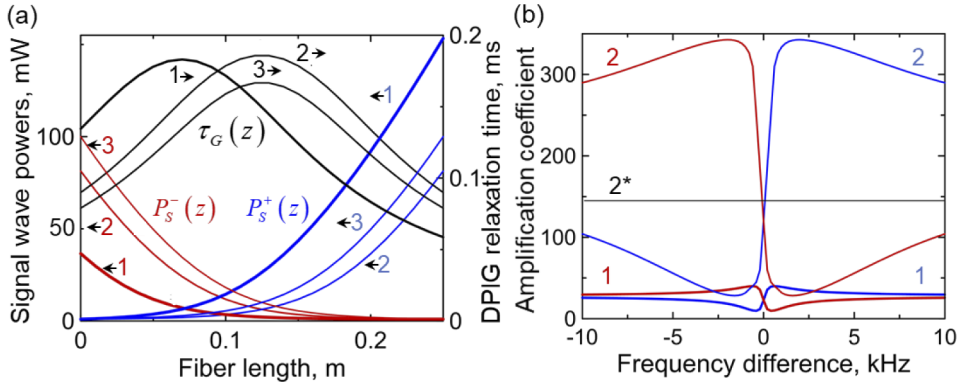

Fig. 4. Steady-state solutions of Eq. (4) for the 25-cm-length pumped fiber. (a) Distributions of the optical signal powers $P_S^+(z)$ (blue), $P_S^-(z)$ (red) and $\tau_g(z)$ (black) along the fiber at $\Delta\omega_S = 3.2\ kHz$;0 and ∞ (curves 1-3), $P_{Pin} = 1.5W$ and $P_S^+(0) = P_S^-(L) = 1\ mW$. (b) The signal amplification coefficients $P_S^+(L)/P_S^+(0)$ (blue curves) and $P_S^-(0)/P_S^-(L)$ (red curves) as functions of the frequency difference $\Delta\omega_S$ at $P_S^+(0) = P_S^-(L) = 1\ mW$ and different pump powers $P_{Pin} = 0.5\ W$; $3\ W$ (curves 1, 2); curve 2* shows the asymptotic level of curve 2 at $\Delta\omega_S \to \infty$.

Optics EXPRESS

Figure 4(b) shows the net amplification achieved for two counterpropagating optical signal as a function of the frequency difference $\Delta\omega_S$. One can see that with two-side pumping at $P_{Pin} = 0.5W$ it exhibits an asymmetric profile with the maximum at $0.7kHz$ and minimum at $-0.5kHz$. The resonance peaks are less pronounced than those shown in Fig. 3 due to an inhomogeneous broadening associated with nonuniform distribution of the grating relaxation time $\tau_G(z)$ over the fiber length shown in Fig. 4(a). However, the key features predicted by the Eqs. (4) are still pronounced. In particular, the positions of spectrum peaks agree with their estimations $\Delta\omega_{SMax}\tilde{\tau}_G \sim 1.4$ and $\Delta\omega_{SMin}\tilde{\tau}_G \sim -0.6$ from Eq. (4) at $\kappa = 2.7$ in such a sense that the corresponding values $\tilde{\tau}_G$ always occurs within the range the $\tau_G(z)$ changes over the fiber length. With an increase of the pump power from $P_{Pin} = 0.5W$ to $P_{Pin} = 3W$ the maximum peak resonant frequency shifts from $0.7kHz$ to $2kHz$ and the minimum peak resonant frequency shifts from $-0.5kHz$ to $-1.6kHz$. These shifts are accompanied by an increase of the peak amplification $P_S^+(L)/P_{Sin}^+$ from 41 to 342 and an increase of the factors B and C from 1.45 to 1.7 and from 3.7 to 11.8, respectively, while the factor A remains at the level of 1.22.

From Fig. 4(b) one can conclude that the power exchange between counterpropagating signals occurs from the wave of lower frequency to the wave of higher frequency. It makes the effect different from Brillouin scattering where the wave at higher frequency commonly donates power to the wave at lower frequency. Formally, this difference can be explained in terms of the sign of refractive index modulation $\delta n(t,z)$ induced by the interference pattern $I(t,z)$ of the interacting signal waves that defines a direction of the energy transfer. The interaction between the counterpropagating optical waves through the modulation $\delta n(t,z)$ is described by Eq. (11) (see, Appendix A). It does not concretize the mechanism of the modulation $\delta n(t,z)$ and, in this sense, is common for BDG and PIDG. In the case of the Brillouin amplification, the acoustic waves (i.e., the waves of density) are produced through the electrostriction effect [5,19,20]: the interference pattern $I(t,z)$ modulates the density forming the acoustic wave amplitude $\xi(t,z) \sim \gamma I(t,z)$. In its tune the acoustic wave amplitude $\xi(t,z)$ modulates the refractive index $\delta n(t,z) \sim \gamma\xi(t,z)$. Importantly both processes are governed by the same electrostrictive coupling constant $\gamma = \xi_0\partial\varepsilon/\partial\xi$, where ε is the dielectric constant and ξ_0 is the media density. Therefore, the effect of $I(t,z)$ on the refractive index $\delta n(t,z) \sim \gamma^2 I(t,z)$ governed by γ^2 is always positive. In contrast, similar exposure $I(t,z)$ in the pumped rare-earth doped fibers reduces the population inversion $\delta g(t,z) \sim -I(t,z)$, whereas $\delta n(t,z) \sim g(t,z)$ is still positive. So, for the BDG $\delta n(t,z) \sim I(t,z)$, but for the PIDG in a pumped rare-earth-doped fiber $\delta n(t,z) \sim -I(t,z)$. The power transfer from the wave at higher frequency to the wave at lower frequency is still available with unpumped rare-earth-doped fibers. Indeed, $P_{P0}^+ = P_{P0}^- = 0$ for the unpumped fibers and the function $\Lambda < 0$ in Eqs. (4), (5). In Eq. (4) the Brillouin-like effect is still described by the third term in brackets, while the second term at $\Lambda < 0$ describes the induced transparency. It is worth noting that the energy conservation law predetermines this formalism. Indeed, in the case of Brillouin scattering, the BDG loses the energy and should be fed by the optical fields. So, the optical domain has to produce the energy converting the light from higher to lower frequency. In the case of PIDG in the pumped fibers, the situation is the opposite. The energy is taken from the population inversion and transferred to the optical domain to increase the grating contrast. So, the optical domain has to spend energy converting the light from lower to a higher frequency. The situation reverses in the case of unpumped fiber.

The similar steady-state solutions shown in Fig. 5 describe the effect of the Brillouin-like amplification in a 1-m-length of unpumped Yb-doped fiber. Figure 5(a) shows typical steady-state power distributions of the interacting waves along the fiber at different values of $\Delta\omega$. The powers of the input optical signals are $P_{Sin}^+ = P_{Sin}^- = 30mW$. The curves calculated at $\Delta\omega = \infty$ describe the transmission of optical signals through the optical amplifier. The observed power absorption occurs independently for two signals due to interaction with Yb-ions in a ground state. Thanks to symmetry of the setup both optical signals starting from the same input power lose the same

Optics EXPRESS

power getting the total transition equal to $P_S^+(L)/P_{Sin}^+ = P_S^-(0)/P_{Sin}^- = 0.72$. Comparing the curves obtained at $\Delta\omega_S = 0$ and $\Delta\omega_S = \infty$ one can see the effect of the induced transparency. The net transmission achieved at $\Delta\omega_S = 0$ $\Delta\omega_S\tau_G$ is ~1.05 times higher (factor A) than that obtained in the case of independent propagation of two waves ($\Delta\omega_S = \infty$). Similar to Fig. 4(a), both curves exhibit strong symmetry in respect to the midpoint of the fiber and $P_S^+(L)/P_{Sin}^+ = P_S^-(0)/P_{Sin}^- = 0.75$. Comparison of the curves obtained at $\Delta\omega_S = 0$ and $\Delta\omega_S/2\pi = 1.5kHz$ (is within the range of ~1.7-1.8 over the fiber length) highlights the Brillouin-like effect providing amplification to the wave at lower frequency at expense of the wave at high frequency. One can see that the output power of the signal at lower frequency is 1.13 times higher than its output power without mutual interaction (at $\Delta\omega_S = \infty$) (factor B) and it is 1.27 times higher than the output power of the signal at higher frequency (factor C). Here, the factors A, B and C characterize the efficiency of the induced transparency (factor A), the Brillouin-like amplification (factor B) and asymmetry of the transmission spectrum (factor C). One can see that with the simulation parameters used and selected $\Delta\omega_S/2\pi = 1.5kHz$, the Brillouin-like amplification is rather weak to compensate completely the optical signal losses in the fiber. However, the effect could be enhanced with a proper selection of $\Delta\omega_S$ and increase of the backward wave power.

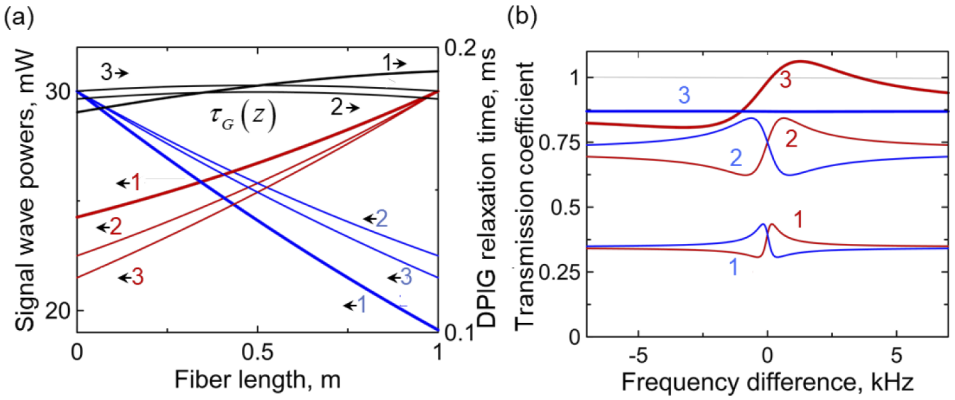

Fig. 5. Steady-state solutions of Eq. (4) for the 1-m-length unpumped fiber. (a) Distributions of the optical signal powers $P_S^+(z)$ (blue), $P_S^-(z)$ (red) and $\tau_g(z)$ (black) along the fiber at $\Delta\omega_S = 1.5\ kHz$;0 and ∞ (curves 1-3) and $P_S^+(0) = P_S^-(L) = 30\ mW$, $P_{Pin} = 0$. (b) The signal transmission $P_S^+(L)/P_S^+(0)$ (blue curves) and $P_S^-(0)/P_S^-(L)$ (red curves) as functions of the frequency difference $\Delta\omega_S$ at $P_S^+(0) = P_S^-(L) = 5\ mW$;$30mW$ (curves 1,2) and $P_S^+(0) = 150mW$, $P_S^-(L) = 1mW$ (curve 3).

Figure 5(b) shows the net transmission achieved for two counterpropagating optical signals as a function of the frequency difference $\Delta\omega_S$. One can see that the transmission of one wave depends on the frequency difference $\Delta\omega_S$ and power of the second wave. With an increase of the second wave power from 5 to $150mW$ the resonant frequency difference shifts from $-0.13Hz$ to $-1.3kHz$ and the peak transmittance for the primary wave increases from 44% to 106%. Thus, the increase of the wave power of lower frequency occurs at expense of the wave power of higher frequency making the effect even more similar to stimulated Brillouin scattering. It is explained by the fact that in the unpumped (Λ<0) rare-earth doped fibers the interference pattern $I(t, z)$ produced by a pair of interacting waves increases the population inversion and, hence, the refractive index in fiber points exposed to higher intensity. So, for the population inversion grating in this case $\delta n(t, z) \sim I(t, z)$, like in the traditional SBS.

Finally, we have performed numerical simulations of the temporal-spatial differential Eq. (3) to explore the formation of the dynamical grating in the pumped rare-earth-doped fiber and

Optics EXPRESS

to analyze evolution of the optical signals to the steady-state solution (Eq. (4)). The fourth-order Runge–Kutta algorithm has been adapted for this purpose. The used initial and boundary conditions are $P_P^+(0,z) = P_P^-(0,z) = P_{Pin}/2; P_S^+(0,z) = P_S^-(0,z) = 0; P_P^+(t,0) = P_P^-(t,L) = P_{Pin}/2$, $P_S^+(t,0) = P_{Sin}^+; P_S^+(t,L) = P_{Sin}^-$. The phases of the input optical signals are constants. The results of this simulations at $\Delta\omega_S = 0$ and $\Delta\omega_S = 3.2\ kHz$ are compared in Fig. 6(a) and (b), respectively. We again consider a 25-cm-length Yb-doped fiber pumped by $P_{Pin} = \sim 1.5W$ from two sides. In both cases, two monochromatic signals with the input powers of ~1mW are introduced into the fiber from the opposite fiber ends. At the moment of time $t = 0$, the forward front of the optical signal wave gets the fiber output possessing the peak output power of $\sim 270mW$ determined by the amplifier transient characteristics. The amplitude of the dynamical grating is close to zero, since the process of the grating inscription is not started yet. Further evolution of the interacting fields depends on the frequency difference $\Delta\omega_S$. At $\Delta\omega_S = 0$ an increase of the grating amplitude caused by the interference pattern leads to suppression of net amplification in the fiber due to hole-burning effect. The output powers of both optical signals decrease down to ~81mW that is by ~ 15mW lower than the steady-state output power at $\Delta\omega_S = \infty$ (see, dashed line for comparison). The typical time of the grating evolution to the steady-state is ~0.1ms. One can see that the phase of the grating complex amplitude $\arg g(t,z)$ monotonically changes over the fiber length due to additional phase shift acquired (through the RIC effect) by the interacting signals $V \approx c\Delta\omega_S/2\tilde{\omega}_S n \sim 1.13cm/s$ during amplification. Importantly, the profile $\arg g(t,z)$ does not change in time at $\Delta\omega_S = 0$. At $\Delta\omega_S = 3.2kHz$ the behavior of the interacting fields is qualitatively different. The dynamical grating is inscribed by the moving interference pattern with the velocity estimated as . In comparison with Fig. 6(a), this feature is reflected in a lower steady-state grating amplitude and longer time of transition to steady-state with recognized re-oscillations shown in the graph of $\max|g(z)|(t)$. The profile $\arg g(t,z)$ still possesses the monotonic change with the fiber length, but also performs weak relaxing perturbations in time of the grating velocity. The dynamical grating moving along the fiber in the positive direction breaks the symmetry and provides preferable amplification of the wave of higher frequency. The steady-state output powers are $\sim 36mW$ and $\sim 154mW$ for the lower and higher frequency waves, respectively. The steady-state distribution $\arg g(z)$ is steeper than the similar distribution at $\Delta\omega_S = 0$. The steady-state solution is well described by Eq. (4).

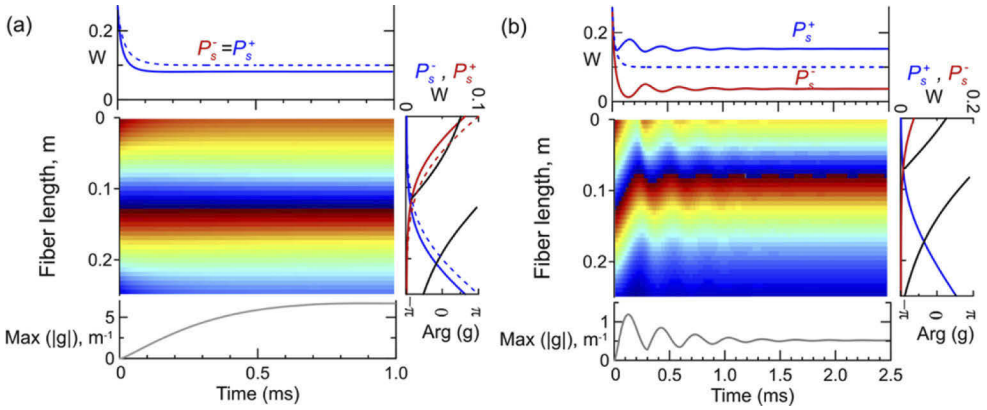

Fig. 6. Evolution of the optical signal powers calculated from Eq. (1) for the 25-cm-length pumped fiber at $\Delta\omega_S = 0$ (a) and $\Delta\omega_S = 3.2\ kHz$ (b). Pump power is $P_{Pin} = 1.5\ W$, input signal powers are $P_S^+(0,t) = P_S^-(0,t) = 1mW$, t>0.

Optics EXPRESS

4. Conclusion

In conclusion, we have described the interaction of two counterpropagating monochromatic waves in a doped optical fiber amplifier demonstrating a strong power transfer from one wave to another. The phenomenon is explained as a reverse effect of the PIDG inscribed by the counterpropagating optical waves in the active fiber. A self-consistent set of equations enabling description of a number of effects governed by the population inversion mechanism, like an optical gain, hole-burning, population inversion grating, laser frequency self-scanning, and so on, is derived and applied to demonstrate the Brillouin-like amplification in rare-earth doped fibers. We have shown that the propagation of the monochromatic wave through the active fiber could provide the wave propagating in the backward direction with an additional gain shifted in frequency by some value in the kHz range. The effect is demonstrated for the configuration of a bidirectional rare-earth-doped optical fiber amplifier. We have shown that in contrast to SBS, the power transfer in the rare-earth-doped fibers could occur either to the wave with higher (anti-Stokes) or lower (Stokes) frequency. Anti-Stokes wave amplification is dominating in the pumped fibers, while amplification of the Stokes wave can occur in fibers without pumping. We believe that the reported Brillouin-like effect could be employed in many new photonics devices expanding the range of the traditional Brillouin applications (fiber lasers, microwave photonics, distributed sensors, spectrometry) to the sub-*kHz* frequency domain. Similar to SBS, the reported narrowband amplitude response is accompanied by a strong dispersive response, able to tailor the phase or group delay of a backward optical signal. In light of these effects, the Brillouin-like amplification could enrich the advanced Brillouin applications such as slow light [32], stored light [33], narrowband RF photonic filters [34], optical processing [4], distributed sensing [35–37], narrowband spectrometers [38], optical amplifiers [39], narrow linewidth, spectrally pure RF sources [40,41] among others. New mechanisms are important as well for designers of the Brillouin and random fiber lasers [42–54] demanded in many applications in microwave photonics, data centers and atomic clocks. Translating the fiber system design to integrated photonics could dramatically reduce the footprint for many these applications.

Appendix

A. Propagation equations for optical waves

The light propagation equation in a rare-earth-doped fiber is derived first. The electric field E is described as [17]:

$$\nabla^2 E - \frac{1}{c^2}\frac{\partial^2}{\partial t^2} n^2 E = 0 \tag{6}$$

where n is the complex refractive index expressed as:

$$n = \left[n_0 - i\frac{\alpha_0}{k^0}\right] + \left[\delta n - i\frac{\delta\alpha}{k^0}\right] \tag{7}$$

where n_0 and α_0 are the refractive index and absorption coefficient of unperturbed fiber, δn and $\delta\alpha$ are the perturbations of the refractive index and absorption coefficient induced by an external pumping of the fiber and interfering optical signals, $k^0 = 2\pi/\lambda_S = \omega_S/c$ is the wave number in vacuum, λ_S and ω_S are the wavelength in vacuum and optical wave frequency.

Under the condition $\frac{\alpha_0}{n_0 k^0} << 1$ underlying the existence of optical wave from Eq. (7):

$$n^2 = {n_0}^2 + 2n_0\left(\delta n - i\frac{(\alpha_0 + \delta\alpha)}{k^0}\right) \tag{8}$$

In a single-mode optical fiber approach [17,27,28], two counterpropagating optical signals with the mode propagation constants $\beta^+ \approx \beta^+ \approx \omega^{\pm} n_0/c$, and the angular oscillation frequency

Optics EXPRESS

ω^+, ω^- are described as a superposition:

$$E_S = F(x,y)\{E_S^+(t,z)e^{i(\omega_S^+ t-\beta_S^+ z)} + E_S^-(t,z)e^{i(\omega_S^- t+\beta_S^- z)} + c.c.\} \tag{9}$$

where $F(x,y)$ is the modal distribution over the fiber cross-section defined from:

$$\left(\frac{\partial^2}{\partial x^2} + \frac{\partial^2}{\partial y^2}\right)F(x,y) + [(k^0 n_0)^2 - (\beta^\pm)^2]F(x,y) = 0 \tag{10}$$

Substituting Eqs. (9), (8) and (10) into Eq. (6), it is reduced to:

$$\begin{aligned}&\left(\beta_1\frac{\partial}{\partial t} + \frac{\partial}{\partial z} + \alpha_0\right)E_S^+ e^{i(\omega_S^+ t-\beta_S^+ z)} + \left(\beta_1\frac{\partial}{\partial t} - \frac{\partial}{\partial z} + \alpha_0\right)E_S^- e^{i(\omega_S^- t+\beta_S^- z)}\\ &= -\left[\left\{\frac{2}{c}\frac{\partial}{\partial t}\left(\delta n - i\frac{\delta\alpha}{k^0}\right) + (ik^0\delta n + \delta\alpha)\right\}[E_S^+ e^{i(\omega_S^+ t-\beta_S^+ z)} + E_S^- e^{i(\omega_S^- t+\beta_S^- z)}]\right]\end{aligned} \tag{11}$$

where $\beta_1 = d\beta_S^\pm/d\omega \approx n_0/c$ is the group velocity dispersion (GVD). We can simplify Eq. (11) using $\partial/\partial t\delta n << \omega_0\delta n$, $\partial/\partial t\delta\alpha << \omega_0\delta\alpha$. Besides, the perturbations of the refractive index δn and absorption coefficient $\delta\alpha$ in Eq. (6) have to be taken into account for two kinds of contributions. The first contribution is associated with the population inversion local gain factor $G(t,z)$ induced in the fiber by an external pumping, the second is due to the PIDG $\delta G(t,z)$ inscribed by two counterpropagating waves. Since both kinds of contributions are governed by the population inversion mechanism, $\delta\alpha$ and δn are strongly linked through the RIC effect (see Eq. (1)). The resulting expressions are $k^0\delta n = \kappa(G+\delta G)/2$, $\delta\alpha = -(G+\delta G)/2$, where κ is defined in Eq. (2). Finally, the light propagation equation in an active fiber reads as

$$\begin{aligned}&\left(\beta_1\frac{\partial}{\partial t} + \frac{\partial}{\partial z} + \alpha_0\right)E_S^+ e^{i(\omega_S^+ t-\beta_S^+ z)} + \left(\beta_1\frac{\partial}{\partial t} - \frac{\partial}{\partial z} + \alpha_0\right)E_S^- e^{i(\omega_S^- t+\beta_S^- z)} =\\ &= \frac{(1-i\kappa)}{2}(G+\delta G)(E_S^+ e^{i(\omega_S^+ t-\beta_S^+ z)} + E_S^- e^{i(\omega_S^- t+\beta_S^- z)})\end{aligned} \tag{12}$$

B. Rate equations for the Gain and Dynamical Gain Gratings

In order to derive equations for the gain and dynamical gain gratings, we start from the standard set of rate equations describing dynamics of the population inversion induced by an external diode pumping and optical signal powers. The model for an effective two-level Yb-doped fiber system (provided that only the fiber core is doped) reads [25]:

$$\begin{aligned}\frac{dN_2(z)}{dt} &= \left(\sigma_{12}^{(p)}\rho_P(0)\frac{P_P(z)}{h\nu_P} + \sigma_{12}^{(s)}\rho_S(0)\frac{P_S(z)}{h\nu_S}\right)N\\ &\quad - \left((\sigma_{21}^{(p)} + \sigma_{12}^{(p)})\rho_P(0)\frac{P_P(z)}{h\nu_P} + (\sigma_{21}^{(s)} + \sigma_{12}^{(s)})\rho_S(0)\frac{P_S(z)}{h\nu_S} + \frac{1}{T}\right)N_2(z)\\ \frac{dP_P(z)}{dz} &= (\sigma_{21}^{(p)} + \sigma_{12}^{(p)})\rho_P(0)P_P(z)N_2(z) - \sigma_{12}^{(p)}\rho_P(0)NP_P(z)\\ \frac{dP_S(z)}{dz} &= (\sigma_{21}^{(s)} + \sigma_{12}^{(s)})\rho_S(0)P_S(z)N_2(z) - \sigma_{12}^{(s)}\rho_S(0)NP_S(z)\end{aligned} \tag{13}$$

Here, P_P and P_S are local powers of pump and signal waves with the frequencies ν_P and ν_S, respectively, at the point z along the fiber length; $\sigma_{12}^{(p)}$ and $\sigma_{21}^{(p)}$ are the effective pump absorption and emission cross sections, $\sigma_{12}^{(s)}$ and $\sigma_{21}^{(s)}$ are the corresponding values for the signal wavelength, $N = 2\pi\int n(r)rdr$ and $N_2 = 2\pi\int n_2(r)rdr$ are the total numbers of all and excited ions integrated over the fiber mode cross-section, respectively;$\rho_P(r)$ and $\rho_S(r)$ are the normalized pump and

Optics EXPRESS

signal power distributions through the fiber cross-section, so that $2\pi \int \rho_{P,S}(r) r dr = 1$; T is the ion excited state life time. For simplicity, we assume the δ-like distribution of the active ions over the fiber cross-section, so $N\rho_S(0) = N_{Yb}$, where N_{Yb} is the concentration of the Yb-ions in the fiber core in accordance with the fiber specification list.

Comparing Eqs. (12) with (13) one can see that

$$G + \delta G = (\sigma_{21}^{(s)} + \sigma_{12}^{(s)})\rho_S(0)N_2(x) \equiv G_T \tag{14}$$

The expression for P_P in Eq. (13) could be rewritten for the case of two-side pumping as:

$$\beta_1 \frac{\partial {P_P}^{\pm}(z)}{\partial t} \pm \frac{\partial {P_P}^{\pm}(z)}{\partial z} = \frac{P_{s0}}{P_{p0}} \frac{\nu_P}{\nu_S} G_T {P_P}^{\pm} - \alpha_p {P_P}^{\pm} \tag{15}$$

where $\alpha_p = \sigma_{12}^{(p)}\rho_P(0)N$, P_{P0}, P_{S0} are the pump and signal saturation powers defined as

$$P_{p0} = \frac{h\nu_p}{T(\sigma_{21}^{(p)} + \sigma_{12}^{(p)})\rho_P(0)}; \qquad P_{s0} = \frac{h\nu_s}{T(\sigma_{21}^{(s)} + \sigma_{12}^{(s)})\rho_S(0)}$$

We can introduce the stimulated transition rates [30] between the ground and excited states:

$$W_p = N\sigma_{12}^{(p)}\rho_S(0)\frac{(\sigma_{21}^{(s)} + \sigma_{12}^{(s)})}{(\sigma_{21}^{(p)} + \sigma_{12}^{(p)})}; \qquad W_s = N\sigma_{12}^{(s)}\rho_S(0) \tag{16}$$

Now, the first equation in Eq. (13) could be rewritten in these terms:

$$T\frac{dG_T}{dt} = \left(W_p \frac{P_P}{P_{P0}} + W_s \frac{P_S}{P_{S0}}\right) - \left(\frac{P_P}{P_{P0}} + \frac{P_S}{P_{S0}} + 1\right) G_T \tag{17}$$

where $P_P \equiv {P_P}^+ + {P_P}^-$; $P_S^+ = E_S^+ E_S^{+*}$; $P_S^- = E_S^- E_S^{-*}$; $q_S = \beta_S^+ + \beta_S^-$; $\Delta\omega_S = \omega_S^+ - \omega_S^-$ and

$$P_S = E_S {E_S}^* = P_S^+ + P_S^- + E_S^+ E_S^{-*}\exp(i(\Delta\omega_S t - q_S z)) + E_S^{+*} E_S^- \exp(-i(\Delta\omega_S t - q_S z)) \tag{18}$$

Equation (18) allows us to separate contributions to $G_T(t, z)$ associated with an external pumping and amplification of two counterpropagating waves.

Since $G_T(t, z)$ is totally real, it can be expressed as:

$$G_T = G + g\ \exp\ (i(\Delta\omega_S t - q_S z)) + g^* \exp(-i(\Delta\omega_S t - q_S z)) \tag{19}$$

where G is the optical gain provided by an external pumping and g is the complex amplitude of the population inversion dynamical grating with the spatial period of $2\pi/|q_S|$. Substituting Eq. (19) into (17), we split Eq. (17) into equations describing the optical gain and gain grating:

$$\begin{aligned} T\frac{dG}{dt} &= \left(W_p \frac{P_P}{P_{P0}} + W_s \frac{P_S}{P_{S0}}\right) - \left(\frac{P_P}{P_{P0}} + \frac{P_S}{P_{S0}} + 1\right) G - \frac{g^* E_S^+ E_S^{-*} + g E_S^{+*} E_S^-}{P_{S0}} \\ T\frac{dg}{dt} &= -\left[\left(\frac{P_P}{P_{P0}} + \frac{P_S}{P_{S0}} + 1 + i\Delta\omega_S T\right) g + (G - W_s)\frac{E_S^+ E_S^{-*}}{P_{S0}}\right] \end{aligned} \tag{20}$$

A self-consistent set of equations Eqs. (3) enabling description of multiple effects (an optical gain, hole-burning, population inversion grating, laser frequency self-scanning) associated with the population inversion mechanism is a combination of Eqs. (12), (19) and (20).

Funding. Ministry of Science and Higher Education of the Russian Federation (#075-15-2021-581); Russian Science Foundation (#18-12-00457P).

Optics EXPRESS

Disclosures. The authors declare no conflicts of interest.

Data availability. Data underlying the results presented in this paper are not publicly available at this time but may be obtained from the authors upon reasonable request

References

1. H. J. Eichler, P. Günter, and D. W. Pohl, *Laser-induced dynamic gratings* (Springer, 2013).
2. A. A. Fotiadi, R. V. Kiyan, and A. Kuzin, "Sbs induced hypersound dynamic grating in multimode optical fibers: Phase conjugation specific features," in *Lasers and Electro-Optics Society Annual Meeting, 1997. LEOS '97 10th Annual Meeting. Conference Proceedings., IEEE*(1997), pp. 44–45 vol.41.
3. K. Y. Song and H. J. Yoon, "Observation of narrowband intrinsic spectra of brillouin dynamic gratings," Opt. Lett. **35**(17), 2958–2960 (2010).
4. M. Santagiustina, S. Chin, N. Primerov, L. Ursini, and L. Thévenaz, "All-optical signal processing using dynamic brillouin gratings," Sci. Rep. **3**(1), 1594 (2013).
5. C. Wolff, M. J. Steel, B. J. Eggleton, and C. G. Poulton, "Stimulated brillouin scattering in integrated photonic waveguides: Forces, scattering mechanisms, and coupled-mode analysis," Phys. Rev. A **92**(1), 013836 (2015).
6. Y. Dong, H. Zhang, D. Zhou, X. Bao, and L Chen., "Characterization of brillouin gratings in optical fibers and their applications," in *Fiber optic sensors* (2012).
7. Z. He and K. Hotate, "Dynamic gratings in optical fibers: Synthesis and sensing applications," Photonic Sens. **2**(1), 60–64 (2012).
8. S. Stepanov, "Dynamic population gratings in rare-earth-doped optical fibres," J. Phys. D: Appl. Phys. **41**(22), 224002 (2008).
9. I. A. Lobach, S. I. Kablukov, E. V. Podivilov, A. A. Fotiadi, and S. A. Babin, "Fourier synthesis with single-mode pulses from a multimode laser," Opt. Lett. **40**(15), 3671 (2015).
10. I. A. Lobach, R. V. Drobyshev, A. A. Fotiadi, E. V. Podivilov, S. I. Kablukov, and S. A. Babin, "Open-cavity fiber laser with distributed feedback based on externally or self-induced dynamic gratings," Opt. Lett. **42**(20), 4207 (2017).
11. A. Budarnykh, I. Lobach, and S. Kablukov, "Self-sweeping tm-doped fiber laser with wavelength stopping," Laser Phys. Lett. **16**(2), 025108 (2019).
12. S. Stepanov, A. Fotiadi, and P. Mégret, "Effective recording of dynamic phase gratings in yb-doped fibers with saturable absorption at 1064 nm," Opt. Express **15**(14), 8832 (2007).
13. E. Aguilar, S. Stepanov, and E. Hernandez, "High-resolution adaptive interferometer with dynamic population grating recorded at 1064 nm in ytterbium-doped fiber," Appl. Opt. **59**(20), 6131–6137 (2020).
14. S. M. Popov, O. V. Butov, A. P. Bazakutsa, M. Y. Vyatkin, Y. K. Chamorovskii, and A. A. Fotiadi, "Random lasing in a short er-doped artificial rayleigh fiber," Results Phys. **16**, 102868 (2020).
15. Y. Bliokh, E. I. Chaikina, I. D. Vatnik, and D. V. Churkin, "Temporal variation of the spectrum of a continuously pumped random fiber laser: Phenomenological model," J. Opt. Soc. Am. B **36**(2), 408–414 (2019).
16. V. V. Spirin, C. A. López-Mercado, D. Kinet, P. Mégret, I. O. Zolotovskiy, and A. A. Fotiadi, "A single-longitudinal-mode brillouin fiber laser passively stabilized at the pump resonance frequency with a dynamic population inversion grating," Laser Phys. Lett. **10**(1), 015102 (2013).
17. G. Agrawal, *Nonlinear fiber optics* (© Academic Press 2001, 2001).
18. B. J. Eggleton, C. G. Poulton, and R. Pant, "Inducing and harnessing stimulated brillouin scattering in photonic integrated circuits," Adv. Opt. Photonics **5**(4), 536–587 (2013).
19. A. L. Gaeta and R. W. Boyd, "Stochastic dynamics of stimulated brillouin scattering in an optical fiber," Phys. Rev. A **44**(5), 3205–3209 (1991).
20. A. Yeniay, J. Delavaux, and J. Toulouse, "Spontaneous and stimulated brillouin scattering gain spectra in optical fibers," J. Lightwave Technol. **20**(8), 1425–1432 (2002).
21. A. A. Fotiadi, R. Kiyan, O. Deparis, P. Mégret, and M. Blondel, "Statistical properties of stimulated brillouin scattering in single-mode optical fibers above threshold," Opt. Lett. **27**(2), 83 (2002).
22. R. Paschotta, J. Nilsson, A. C. Tropper, and D. C. Hanna, "Ytterbium-doped fiber amplifiers," IEEE J. Quantum Electron. **33**(7), 1049–1056 (1997).
23. A. A. Fotiadi, O. L. Antipov, and P. Mégret, "Dynamics of pump-induced refractive index changes in single-mode yb-doped optical fibers," Opt. Express **16**(17), 12658 (2008).
24. A. Fotiadi, O. Antipov, M. Kuznetsov, and P. Mégret, "Refractive index changes in rare earth-doped optical fibers and their applications in all-fiber coherent beam combining," in *Coherent laser beam combining*(2013), pp. 193–230.
25. H. Pask, R. J. Carman, D. C. Hanna, A. C. Tropper, C. J. Mackechnie, P. R. Barber, and J. M. Dawes, "Ytterbium-doped silica fiber lasers: Versatile sources for the 1-1.2/spl mu/m region," IEEE J. Sel. Top. Quantum Electron. **1**(1), 2–13 (1995).
26. S. K. Turitsyn, A. E. Bednyakova, M. P. Fedoruk, A. I. Latkin, A. A. Fotiadi, A. S. Kurkov, and E. Sholokhov, "Modeling of cw yb-doped fiber lasers with highly nonlinear cavity dynamics," Opt. Express **19**(9), 8394 (2011).
27. L. Mescia, "Design of long-period gratings in cladding-pumped microstructured optical fiber," J. Opt. Soc. Am. B **25**(11), 1833–1839 (2008).
28. F. Prudenzano, L. Mescia, T. Palmisano, M. Surico, M. De Sario, and G. C. Righini, "Optimization of pump absorption in mof lasers via multi-long-period gratings: Design strategies," Appl. Opt. **51**(9), 1420–1430 (2012).

Optics EXPRESS

29. A. A. Fotiadi, G. Brambilla, T. Ernst, S. A. Slattery, and D. N. Nikogosyan, "Tpa-induced long-period gratings in a photonic crystal fiber: Inscription and temperature sensing properties," J. Opt. Soc. Am. B **24**(7), 1475–1481 (2007).
30. M. Aubry, L. Mescia, A. Morana, T. Robin, A. Laurent, J. Mekki, E. Marin, Y. Ouerdane, S. Girard, and A. Boukenter, "Temperature influence on the radiation responses of erbium-doped fiber amplifiers," Phys. Status Solidi A **218**(15), 2100002 (2021).
31. R. Paschotta, J. Nilsson, L. Reekie, A. C. Trooper, and D. C. Hanna, "Single-frequency ytterbium-doped fiber laser stabilized by spatial hole burning," Opt. Lett. **22**(1), 40–42 (1997).
32. L. Thévenaz, "Slow and fast light in optical fibres," Nat. Photonics **2**(8), 474–481 (2008).
33. M. Merklein, B. Stiller, and B. J. Eggleton, "Brillouin-based light storage and delay techniques," J. Opt. **20**(8), 083003 (2018).
34. D. Marpaung, B. Morrison, M. Pagani, R. Pant, D.-Y. Choi, B. Luther-Davies, S. J. Madden, and B. J. Eggleton, "Low-power, chip-based stimulated brillouin scattering microwave photonic filter with ultrahigh selectivity," Optica **2**(2), 76–83 (2015).
35. A. Bergman, T. Langer, and M. Tur, "Coding-enhanced ultrafast and distributed brillouin dynamic gratings sensing using coherent detection," J. Lightwave Technol. **34**(24), 5593–5600 (2016).
36. H. Zhang, D. Zhou, B. Wang, C. Pang, P. Xu, T. Jiang, D. Ba, H. Li, and Y. Dong, "Recent progress in fast distributed brillouin optical fiber sensing," Appl. Sci. **8**(10), 1820 (2018).
37. J. L. Bueno Escobedo, J. Jason, C. A. López-Mercado, V. V. Spirin, M. Wuilpart, P. Mégret, D. A. Korobko, I. O. Zolotovskiy, and A. A. Fotiadi, "Distributed measurements of vibration frequency using phase-otdr with a dfb laser self-stabilized through pm fiber ring cavity," Results Phys. **12**, 1840–1842 (2019).
38. Y. Dong, T. Jiang, L. Teng, H. Zhang, L. Chen, X. Bao, and Z. Lu, "Sub-mhz ultrahigh-resolution optical spectrometry based on brillouin dynamic gratings," Opt. Lett. **39**(10), 2967–2970 (2014).
39. S. M. Raupach, A. Koczwara, and G. Grosche, "Brillouin amplification supports 1× 10− 20 uncertainty in optical frequency transfer over 1400 km of underground fiber," Phys. Rev. A **92**(2), 021801 (2015).
40. L. McKay, M. Merklen, Y. Liu, A. Cramer, J. Maksymow, A. Chilton, K. Yan, D.-Y. Choi, S. J. Madden, R. DeSalvo, and B. J. Eggleton, "Integrated microwave photonic true-time delay with interferometric delay enhancement based on brillouin scattering and microring resonators," Opt. Express **28**(24), 36020–36032 (2020).
41. Q. Jia, P. Zhang, T. Wang, X. Li, and B. Bo, "40 ghz narrow linewidth frequency-switched microwave signal generation based on a single-longitudinal-mode double-brillouin-frequency spaced brillouin fiber laser," Appl. Opt. **56**(19), 5323–5328 (2017).
42. A. A. Fotiadi and R. V. Kiyan, "Cooperative stimulated brillouin and rayleigh backscattering process in optical fiber," Opt. Lett. **23**(23), 1805 (1998).
43. A. S. L. Gomes, A. L. Moura, C. B. de Araújo, and E. P. Raposo, "Recent advances and applications of random lasers and random fiber lasers," Prog. Quantum Electron. **78**, 100343 (2021).
44. Z. Zhou, L. Chen, and X. Bao, "High efficiency brillouin random fiber laser with replica symmetry breaking enabled by random fiber grating," Opt. Express **29**(5), 6532–6541 (2021).
45. M. A. Arshad, A. Hartung, A. C. Pratiwi, and M. Jäger, "Observation of direction instability in a fiber ring laser," Sci. Rep. **11**(1), 4436 (2021).
46. V. V. Spirin, J. L. Bueno Escobedo, S. V. Miridonov, M. C. Maya Sánchez, C. A. López-Mercado, D. A. Korobko, I. O. Zolotovskii, and A. A. Fotiadi, "Sub-kilohertz brillouin fiber laser with stabilized self-injection locked dfb pump laser," Opt. Laser Technol. **141**, 107156 (2021).
47. A. Tehranchi, V. L. Iezzi, and R. Kashyap, "Power fluctuations and random lasing in multiwavelength brillouin erbium-doped fiber lasers," J. Lightwave Technol. **37**(17), 4439–4444 (2019).
48. Y. Song, S. Li, J. Zhang, M. Zhang, L. Qiao, and T. Wang, "The modeling of random brillouin dynamic grating," Opt. Fiber Technol. **53**, 102034 (2019).
49. V. V. Spirin, J. L. Bueno Escobedo, D. A. Korobko, P. Mégret, and A. A. Fotiadi, "Dual-frequency laser comprising a single fiber ring cavity for self-injection locking of dfb laser diode and brillouin lasing," Opt. Express **28**(25), 37322–37333 (2020).
50. J. Deng, M. Han, Z. Xu, Y. Du, and X. Shu, "Stable and low-threshold random fiber laser via anderson localization," Opt. Express **27**(9), 12987–12997 (2019).
51. S. M. Popov, O. V. Butov, Y. K. Chamorovski, V. A. Isaev, P. Mégret, D. A. Korobko, I. O. Zolotovskii, and A. A. Fotiadi, "Narrow linewidth short cavity brillouin random laser based on bragg grating array fiber and dynamical population inversion gratings," Results Phys. **9**, 806–808 (2018).
52. W. Margulis, A. Das, J. P. von der Weid, and A. S. L. Gomes, "Hybrid electronically addressable random fiber laser," Opt. Express **28**(16), 23388–23396 (2020).
53. E. K. Kashirina, I. A. Lobach, and S. I. Kablukov, "Dual-longitudinal-mode cw self-sweeping operation in er-doped fiber laser," Opt. Lett. **45**(24), 6659–6662 (2020).
54. R. V. Drobyshev, N. R. Poddubrovskii, I. A. Lobach, and S. I. Kablukov, "High-resolution spectral analysis of long single-frequency pulses generated by a self-sweeping yb-doped fiber laser," Laser Phys. Lett. **18**(8), 085102 (2021).